Madden–Julian Oscillation–Induced Suppression of Northeast Pacific Convection Increases U.S. Tornadogenesis

DONGMIN KIM

Cooperative Institute for Marine and Atmospheric Studies, University of Miami, and NOAA/Atlantic Oceanographic and Meteorological Laboratory, Miami, Florida

SANG-KI LEE AND HOSMAY LOPEZ

NOAA/Atlantic Oceanographic and Meteorological Laboratory, Miami, Florida

(Manuscript received 26 December 2019, in final form 9 March 2020)

ABSTRACT

This study investigates the impact of the Madden–Julian oscillation (MJO) on U.S. tornadogenesis using atmospheric reanalysis and model experiments. Our analysis shows that the impact of MJO on U.S. tornadogenesis is most significant in May–July and during MJO phases 3–4 and 5–6 (P3456). These MJO phases are characterized by anomalous ascending motion over the Maritime Continent (MC) and anomalous subsidence over the northeast Pacific (EP), generating anomalous diabatic heating and cooling, respectively. These in turn generate large-scale atmospheric conditions conducive to tornadogenesis in the United States, enhancing the North American low-level jet (NALLJ) and thus increasing the influx of warm and moist air from the Gulf of Mexico to the United States and increasing the low-level wind shear and convective available potential energy along its path. Conversely, during MJO phases 1–2 and 7–8, the opposite patterns of atmospheric anomalies appear over the United States producing unfavorable environments for U.S. tornadogenesis. We further investigate the underlying mechanism for MJO-induced atmospheric circulations conducive to U.S. tornadogenesis using a linear baroclinic model (LBM). The LBM is forced by diabatic heating over the MC and cooling over the EP, which characterizes the P3456 MJO phase. The model experiment reproduces an anomalous ridge over the southern United States and associated anomalous low-level anticyclone that enhances the NALLJ and increases tornadic environmental parameters. Additional sensitivity experiments prescribing the diabatic heating over the MC and diabatic cooling over the EP independently demonstrate that diabatic cooling over the EP is the main driver for producing regional atmospheric conditions favorable for U.S. tornadogenesis.

1. Introduction

The National Oceanic and Atmospheric Administration's Storm Prediction Center (NOAA SPC) provides a 1–8-day lead-time severe weather forecast, including tornado watches. This severe weather forecast is based on synoptic-scale atmospheric instability [e.g., convective available potential energy (CAPE) and low-level wind shear (LLWS)] from numerical weather forecast models and observations. To extend the current forecast lead time for tornadogenesis to subseasonal time scales (i.e., 14–30 days of lead time), several studies have explored a potential link between U.S. tornado activity and the Madden–Julian oscillation (MJO; Madden and Julian 1972), which is defined by the convective activity over the Maritime Continent propagating eastward around the equatorial tropics with a 30–90-day period (e.g., Thompson and Roundy 2013; Barrett and Gensini 2013; Barrett and Henley 2015; Gensini and Marinaro 2016; Tippett 2018; Baggett et al. 2018; Moore and McGuire 2020; Gensini et al. 2019).

Thompson and Roundy (2013) found that in March–May, the chances of violent tornado outbreaks in the United States are maximized during MJO phase 2, when the convection over the Indian Ocean is enhanced (Fig. 1c). Barrett and Gensini (2013) showed that the relationship between the MJO and U.S. tornado activity may differ between April and May, with increased frequency of tornado days during MJO phases 6 and 8 in April and MJO phases 5 and 8 in May. On the other

Corresponding author: Dr. Dongmin Kim, dongmin.kim@noaa.gov

DOI: 10.1175/JCLI-D-19-0992.1

© 2020 American Meteorological Society. For information regarding reuse of this content and general copyright information, consult the AMS Copyright Policy (www.ametsoc.org/PUBSReuseLicenses).

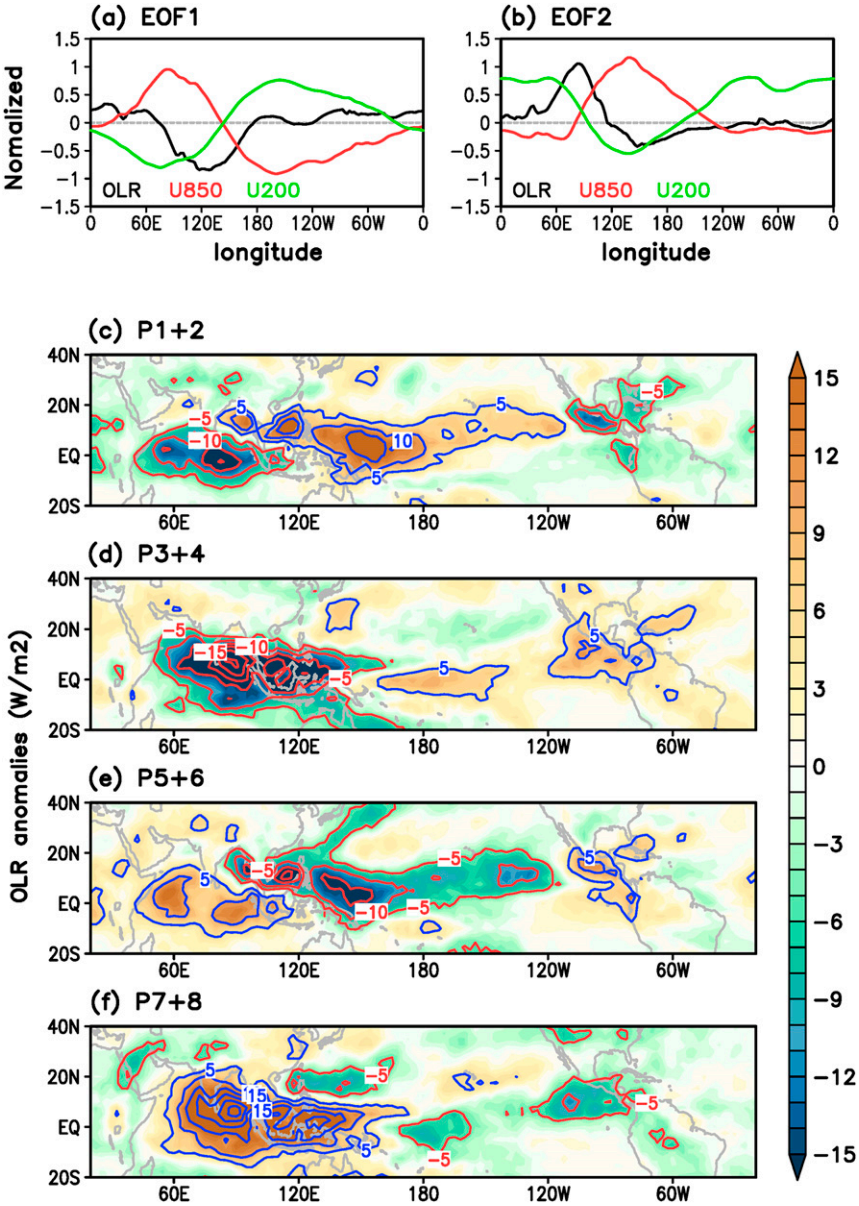

FIG. 1. (top) Spatial structure of (a) EOF1 and (b) EOF2 in combined EOF analysis using NOAA interpolated OLR (black lines) and zonal wind at 850 (red lines) and 200 hPa (green lines) from NCEP2 during 1979–2016. (bottom) OLR composite maps during MJJ for (c) MJO phases 1+2, (d) MJO phases 3+4, (e) MJO phases 5+6, and (f) MJO phases 7+8. Red contours indicate negative OLR anomalies $\leq -5\,\mathrm{W\,m^{-2}}$ and blue contours indicate positive OLR anomalies $\geq +5\,\mathrm{W\,m^{-2}}$.

hand, Tippett (2018) showed that the number of tornado days is significantly reduced only during MJO phases 5–8 in April, and that there is no robust relationship between the MJO and U.S. tornado activity during other MJO phases or in other months.

Recent studies also explored the impact of interactive relationship between MJO and global wind oscillation (GWO), which is defined by the global atmospheric angular momentum, on the U.S. tornado activity (Gensini et al. 2019; Moore and McGuire 2020). Moore and McGuire (2020), for instance, explored the interactive impact of GWO and MJO on U.S. tornado days during different seasons. Additionally, Gensini et al. (2019) suggested that MJO and GWO events can produce favorable atmospheric conditions for U.S. tornadic storms in the United States.

Baggett et al. (2018) further showed useful forecast skills of the MJO-induced tornadic environmental parameters (i.e., CAPE and low-level storm relative helicity) within 45-day lead time using the MJO index. These results suggested that the MJO can be used as a potential predictor for U.S. tornado activity at subseasonal time scales, given that the current generation of climate forecast models have a reliable forecast skill of the MJO up to around 40 days (e.g., Lee et al. 2014; Vitart 2017; Kim et al. 2018).

Based on recent studies, there is clear evidence that U.S. tornado activity is increased during certain phases of the MJO. However, it should be noted that the relationship between U.S. tornado activity and the MJO shown in these studies is largely based on statistical analyses; thus, the physical mechanism underlying the relationship between the MJO and tornadic environmental parameters is not yet fully understood. Therefore, the main objective of this study is to examine the atmospheric dynamics responsible for the relationship between the MJO and U.S. tornadogenesis. To achieve this objective, we first carry out composite analyses of the atmospheric conditions associated with various phases of the MJO in May–July (MJJ), during which the relationship between MJO and U.S. tornadogenesis is robust, using atmospheric reanalysis products and observations (sections 3b–d). Based on the composite analysis, we propose a hypothesis that the suppressed convection over the northeast Pacific during the MJO phases 3-4-5-6 is the key process that forces regional atmospheric circulation anomalies conducive to U.S. tornadogenesis. Then, we further demonstrate our working hypothesis using a linear baroclinic model (LBM) with idealized diabatic forcing patterns (section 3e).

2. Data, methods, and model experiments

The MJO is diagnosed by a combined empirical orthogonal function (EOF) using NOAA's meridionally averaged (5°S–5°N) daily interpolated outgoing longwave radiation (OLR) dataset (Liebmann and Smith 1996) and the zonal winds at 850 and 200 hPa from National Centers for Environmental Prediction reanalysis, version 2 (NCEP2; Kanamitsu et al. 2002). To obtain subseasonal anomalies, we first remove climatological seasonal cycle for the period 1979–2016. Then, we subtract the 120-day moving averages of the anomalous OLR and zonal winds. This method has been used in many previous MJO studies (e.g., Wheeler and Hendon 2004; Kim et al. 2014).

To perform composite analysis for specific MJO phases, we calculate the Real-time Multivariate MJO (RMM) index as defined by Wheeler and Hendon (2004). To ensure robust results, only strong MJO events (i.e., RMM $\geq$ 1.0) are selected in this study, as in previous MJO–U.S. tornadoes studies (e.g., Thompson and Roundy 2013; Barrett and Gensini 2013). For global composite analysis, we use anomalous OLR from NOAA's interpolated OLR dataset, divergent winds at 200 hPa, geopotential height at 500 hPa, and winds at 850 hPa from NCEP2. The North American Regional Reanalysis (NARR; Mesinger et al. 2006) is also used to explore the relationship between MJO and tornadic environmental parameters (i.e., surface-based CAPE and LLWS between 850 and 1000 hPa) over the United States. Similarly, for the definition of the MJO index, the seasonal cycle and 120-day running mean are removed from each variable in order to isolate the subseasonal variability.

The U.S. tornado dataset is obtained from the Severe Weather Database (SWD) of NOAA SPC for the study period of 1979–2016. Tornado intensity is classified by the wind speed and damage using the Fujita (F) and enhanced Fujita (EF) scales (Doswell et al. 2009). These scales are ranked from 0 to 5 according to the observed damage. To avoid a spurious long-term trend in the tornado dataset, we only count the number of tornadoes reported to F and EF scales greater than or equal to 1 (EF1–5; Verbout et al. 2006; Lee et al. 2016) only during strong MJO events. The MJO-related tornadogenesis are calculated by the deviation from the long-term averaged tornadogenesis for each of the eight MJO phases for each calendar month. To examine the spatial distribution of EF1–5 tornadogenesis, EF1–5 tornadoes are counted for each of the 1° × 1° grid points over the contiguous United States.

We also use an LBM (Watanabe and Kimoto 1999) to demonstrate the impact of MJO on the atmospheric large-scale circulation conducive to U.S. tornadogenesis. The LBM is a primitive-equation model linearized under a basic state and is a valuable tool to diagnose anomalous atmospheric circulations forced by regional diabatic heating or Rossby wave sources (e.g., Hoskins and Simmons 1975; Ting and Held 1990; Watanabe and Kimoto 1999; Lee et al. 2009; Lopez et al. 2019). The LBM is integrated at a T21 horizontal resolution (~5.5° latitude) and five vertical levels in sigma coordinates (T21L5). We use the steady-state solution using the matrix inversion technique (Hoskins and Karoly 1981; Watanabe and Kimoto 1999). Further detailed information about the LBM is well documented in Watanabe and Kimoto (1999).

3. Results

a. *Characteristics of MJO and its convective activity*

Figures 1a and 1b show the zonal structure of the combined EOF1 and EOF2 for the study period

(1979–2016), explaining 11.89% and 11.39% of the total variance, respectively. The zonal structure of EOF1 shows the convective center, as indicated by anomalous negative OLR, low-level convergence, and upper-level divergence, over the Maritime Continent (~120°E). The zonal structure of EOF2 illustrates the eastward propagation of the convective center toward the western Pacific warm pool (~150°E). These zonal structures of the two EOF modes are typical patterns of MJO cycle shown in previous studies (e.g., Wheeler and Hendon 2004; Kim et al. 2014). We further explore spatial patterns of OLR anomalies during MJJ for the MJO phases 1+2, 3+4, 5+6, and 7+8 (Figs. 1c–f). The negative OLR anomalies start over the Indian Ocean (MJO phases 1+2) and propagate eastward through the Maritime Continent (MJO phases 3+4). The convective center moves northeastward over the western North Pacific and passes across the date line (MJO phases 5+6), followed by a suppression of convection in the Indian Ocean (MJO phases 7+8). These patterns of OLR anomalies for different MJO phases are consistent with previous studies (e.g., Kemball-Cook and Wang 2001; Lawrence and Webster 2002; Kim et al. 2014) and also are known to affect spatiotemporal variations of U.S. tornadogenesis (e.g., Thompson and Roundy 2013; Barrett and Gensini 2013; Barrett and Henley 2015; Tippett 2018; Baggett et al. 2018; Moore and McGuire 2020; Gensini et al. 2019). We further explore the relationship between MJO and spatiotemporal U.S. tornadogenesis in the next section.

b. *Characteristics of the MJO-related U.S. tornadogenesis*

Figure 2 shows the MJO-related EF1–5 tornadogenesis over the United States for 38 years (1979–2016), stratified by calendar month. The number of days for strong MJO (RMM index ≥ 1.0) is 8482 days out of a total of 13 880 days (61.1%). The total number of MJO-related EF1–5 tornadoes occurring during the strong MJO periods is about 11 656 cases out of a total of 28 639 cases (40.9%). As shown in Fig. 2, the MJO-related tornadogenesis over the United States exhibits a strong seasonal dependency, consistent with Tippett (2018) and Moore and McGuire (2020). For instance, U.S. tornadogenesis between August and February is largely insensitive to MJO phases. However, in March, the maximized MJO-related tornadogenesis occurs during MJO phase 2, in agreement with Thompson and Roundy (2013) and Tippett (2018), whereas in April the U.S. tornadogenesis is more frequent during the MJO phases 5 and 8, and less frequent during MJO phases 3 and 4, consistent with Barrett and Gensini (2013). However, as clearly shown in Fig. 2, the relationship between MJO

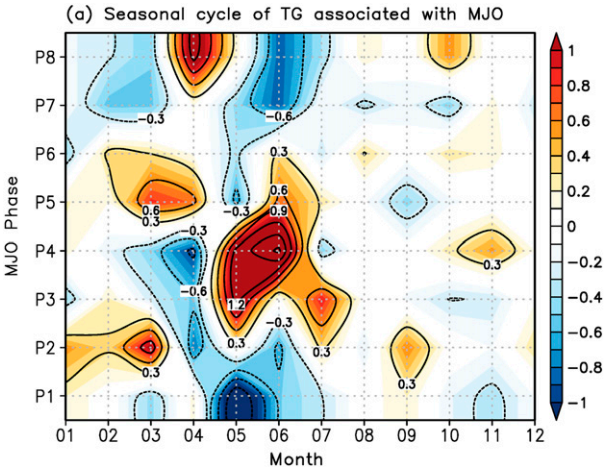

FIG. 2. Seasonal cycle of the EF1–5 tornadogenesis anomalies (tornadogenesis per day) over the United States associated with MJO phases for 38 years (1979–2016). The tornadogenesis anomalies are taken from averaged tornadogenesis in all MJO phases for each month.

and U.S. tornadogenesis is much more robust in late spring and early summer (i.e., MJJ) compared to early and midspring (i.e., March and April). In MJJ, U.S. tornadogenesis greatly increases during MJO phases 3-4-5-6 (P3456) and decreases during MJO phases 1-2-7-8 (P1278). Therefore, in this study, we explore the impacts of the MJO on U.S. tornadogenesis and the associated atmospheric circulations focusing on MJJ.

Figure 3a shows the spatial distribution of the MJO-induced U.S. tornadogenesis during MJJ. Tornadogenesis is maximized over the southern United States, particularly Texas and Oklahoma. Over the western United States, west of 110°W, tornadogenesis is negligible. This spatial pattern is consistent with the spatial pattern of climatological U.S. tornadogenesis during MJJ (not shown). Figure 3b shows the spatial pattern of the peak MJO phases for U.S. tornadogenesis, which is defined by the MJO phase during which the largest number of tornadogenesis occurs in MJJ. Overall, the dominant MJO phases for U.S. tornadogenesis are MJO P3456 (red and green dots in Fig. 3b), which are linked to anomalous convection over the Maritime Continent and western Pacific warm pool (Figs. 1d,e). Those are consistent with our result that the U.S. tornadogenesis increases greatly during MJO P3456 (Fig. 2). Interestingly, the peak MJO phases of tornadogenesis are clustered in two different regions in the United States. Specifically, tornadogenesis is more frequent over the South and the Ohio Valley during MJO P34, and over the Southeast and the Northeast during MJO P56. We further discuss this topic in section 3d. To better understand the link between

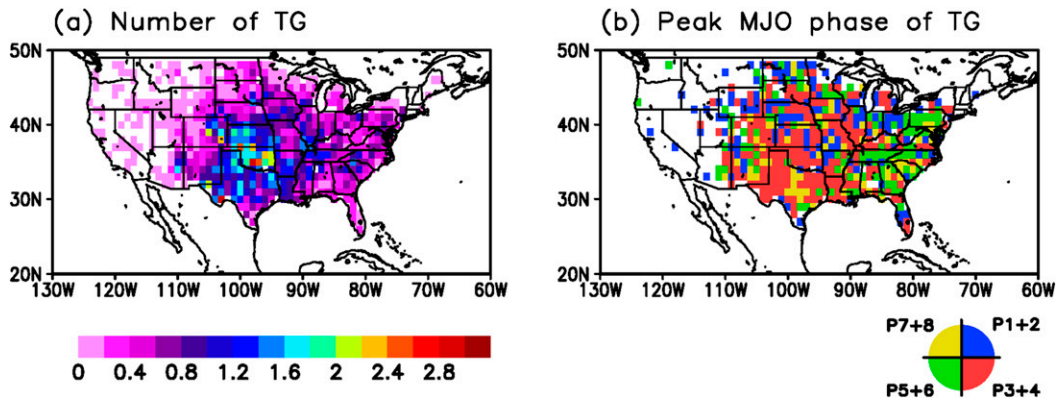

FIG. 3. (a) Spatial distribution of the MJO-related U.S. tornadogenesis in MJJ (tornadogenesis per day) and (b) the peak MJO phases of the most frequent U.S. tornadogenesis occurrence in MJJ.

MJO phases and spatial distribution of U.S. tornadogenesis shown in Fig. 3b, we then examine the MJO-induced atmospheric circulation anomalies and associated tornadic environmental parameters that influence U.S. tornadogenesis.

c. *MJO-induced large-scale atmospheric anomalies and their impacts on the U.S. tornadic environmental parameters*

We explore composite maps of OLR, upper-level (200 hPa) divergence and velocity potential anomalies during MJO P1278 and MJO P3456, which indicate inactive and active MJO phases for U.S. tornadogenesis, respectively. During MJO P1278, strong positive OLR and upper-level convergence anomalies appear over the Maritime Continent and compensating negative OLR and upper-level divergence anomalies appear over the northeast Pacific (5°–20°N, 70°–110°W) as shown in Fig. 4a. The opposite patterns occur during MJO P3456, with negative OLR and upper-level divergence anomalies over the Maritime Continent (Fig. 4b). These two composite maps for MJO P1278 and MJO P3456 are consistent with those shown in earlier studies (e.g., Wheeler and Hendon 2004; Zhang and Dong 2004; Kim et al. 2014).

Figure 4c illustrates 500-hPa geopotential height anomalies and low-level (850 hPa) wind anomalies during MJO P1278. During MJO P1278, anomalous westerly winds prevail over the tropical Pacific, and anomalous easterly winds over the tropical Indian Ocean, consistent with the anomalous upper-level convergence over the Maritime Continent and divergence over the northeast Pacific. A strong midlevel anomalous atmospheric trough appears over the North Pacific, north of 30°N. Additionally, a paired anomalous atmospheric ridge and trough appear across North America. The anomalous trough centered over the southern United States promotes low-level northerly wind anomalies over the central United States, and thus weakens the North American low-level jet (NALLJ; Wang and Fu 2004) that supplies warm and moist low-level air from the Gulf of Mexico (GoM) to the central United States. In contrast, during MJO P3456 (Fig. 4d), anomalous easterly winds prevail over the tropical Pacific, and anomalous westerly winds over the tropical Indian Ocean, consistent with the anomalous upper-level divergence over the Maritime Continent. A strong midlevel anomalous atmospheric ridge appears over the North Pacific, strengthening the North Pacific subtropical high. A paired anomalous atmospheric trough and ridge appears across North America. The anomalous ridge centered over the southern United States produces low-level southerly wind anomalies over the central United States, thus reinforces the NALLJ.

Figure 5 shows the composite maps of CAPE, LLWS, low-level winds (850 hPa) and vertically integrated water vapor fluxes during MJO P1278 and P3456, derived from NARR. During MJO P1278, low-level northerly wind anomalies prevail over the United States, consistent with the results from NCEP2 (Fig. 4b). The low-level northerly wind anomalies weaken the NALLJ, and thus decrease the warm and moist fluxes from the GoM into the central United States. These anomalies also reduce the LLWS and CAPE over the United States, stabilizing the atmosphere over the United States and reducing U.S. tornadogenesis (Figs. 5a,c). During MJO P3456, on the other hand, low-level southerly wind anomalies predominate over the central United States, reinforcing the NALLJ. The enhanced NALLJ increases LLWS and CAPE, and destabilize the atmosphere over the United States (Figs. 5b,d). These conditions are favorable for U.S. tornadogenesis as documented in previous studies (e.g., Doswell and Bosart 2001; Weaver et al. 2012; Lee et al. 2013, 2016; Barrett and Gensini 2013; Allen et al. 2015; Lepore et al. 2017; Baggett et al. 2018; Molina et al. 2018; Molina and Allen 2019).

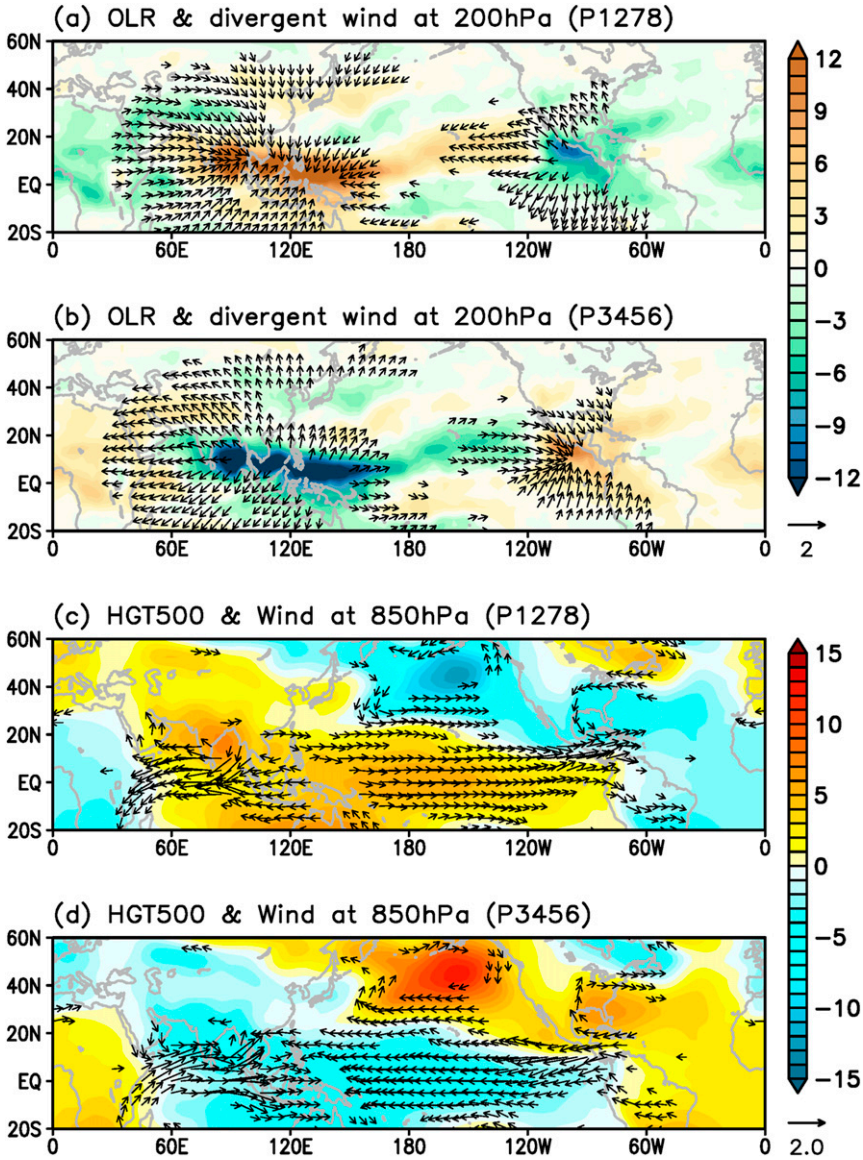

FIG. 4. Composite maps of the anomalous outgoing longwave radiation (shaded; W m^{-2}) and divergent winds at 200 hPa (vectors; m s^{-1}; omitted below 0.5 m s^{-1}) during (a) MJO P1278 and (b) MJO P3456. (c),(d) As in (a) and (b), but for anomalous geopotential height at 500 hPa (shaded; gpm) and wind anomalies at 850 hPa (vectors; m s^{-1}; omitted below 0.5 m s^{-1}). The results are derived from NCEP2.

In summary, the composite analysis demonstrates that the MJO-related large-scale atmospheric circulation anomalies modulate the synoptic-scale tornadic environmental parameters (i.e., LLWS and CAPE) over the United States. More specifically, during MJO P3456, anomalous ascending and descending motions appear over the Maritime Continent and the northeast Pacific, respectively. In addition, an anomalous midlevel atmospheric ridge appears over the southern United States, which in turn strengthens the NALLJ. The strengthened NALLJ further increases LLWS and CAPE over the central United States and thus increases U.S. tornadogenesis. On the other hand, the MJO P1278 produces opposite patterns of atmospheric circulation anomalies and thus weakens the NALLJ and decreases U.S. tornadogenesis.

d. U.S. tornadic environmental parameters during MJO P34 versus MJO P56

Interestingly, the peak MJO phase for U.S. tornadogenesis is divided into two clusters: MJO P34 west of 90°W and MJO P56 east of 90°W, as shown in Fig. 3b.

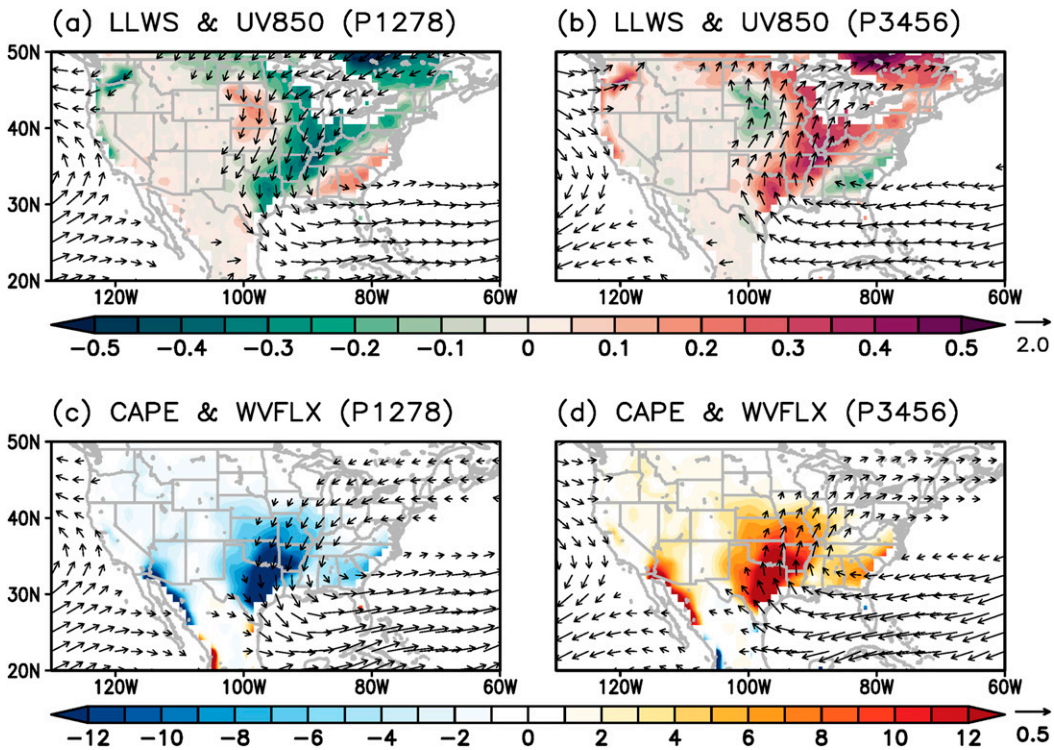

FIG. 5. Composite maps of the anomalous low-level wind shear (shaded; $m\,s^{-1}$) and wind anomalies at 850 hPa (vectors; $m\,s^{-1}$; omitted below $0.5\,m\,s^{-1}$) during (a) MJO P1278 and (b) MJO P3456. (c),(d) As in (a) and (b), but for the anomalous convective available potential energy (CAPE; shaded; $J\,kg^{-1}$) and anomalous vertical integrated water vapor flux (vectors; $kg\,m^{-1}\,s^{-1}$; omitted below $0.1\,kg\,m^{-1}\,s^{-1}$). The results are derived from NARR.

More specifically, tornadogenesis is more frequent over the South and the Ohio Valley during MJO P34 (red color in Fig. 3b), whereas the Southeast and the Northeast are more impacted during MJO P56 (green color in Fig. 3b). This result suggests that the MJO affects not only the number of U.S. tornadogenesis events but also the spatial pattern of tornadogenesis over the United States.

As shown in Figs. 6a and 6c, the low-level wind anomalies and moisture flux from the GoM are enhanced over the South and the Ohio Valley (i.e., southerly anomalies), but reduced over the Southeast (i.e., easterly anomalies) during MJO P34. Consistently, LLWS and CAPE are increased over the South and the Ohio Valley, but decreased over the Southeast. During MJO P56, in contrast, the low-level wind anomalies strengthen and shift eastward toward the Southeast and the Northeast. Due to the eastward shift in the low-level wind anomalies, the area of increased LLSW, CAPE, and moisture flux is displaced eastward to the Southeast and the Northeast (Fig. 6b). These patterns of tornadic environmental parameters nicely explain why U.S. tornadogenesis is increased in the South and the Ohio Valley during MJO P34 and in the Southeast and the Northeast during MJO P56.

e. The physical mechanism underlying the MJO control of U.S. tornadogenesis

As investigated in previous studies (e.g., Moon et al. 2011; Becker et al. 2011; Zhou et al. 2012; Henderson et al. 2017), the MJO-induced extratropical Rossby wave propagation, which influences U.S. weather and climate variations (e.g., Becker et al. 2011; Zhou et al. 2012), is prominent during boreal winter when the Pacific jet stream is stronger and shifted equatorward. However, as shown in Fig. 2, the relationship between MJO phase and U.S. tornadogenesis is most robust during MJJ when the extratropical Rossby wave propagation associated with the MJO is not vigorous. This suggests that the MJO-induced extratropical Rossby wave propagation may not be the key factor modulating U.S. tornadogenesis during MJJ. Therefore, it is important to understand the seasonality of the MJO and MJO-induced atmospheric circulation anomalies.

In boreal winter, the MJO signal is largely confined to the Maritime Continent (e.g., Wheeler and Hendon 2004;

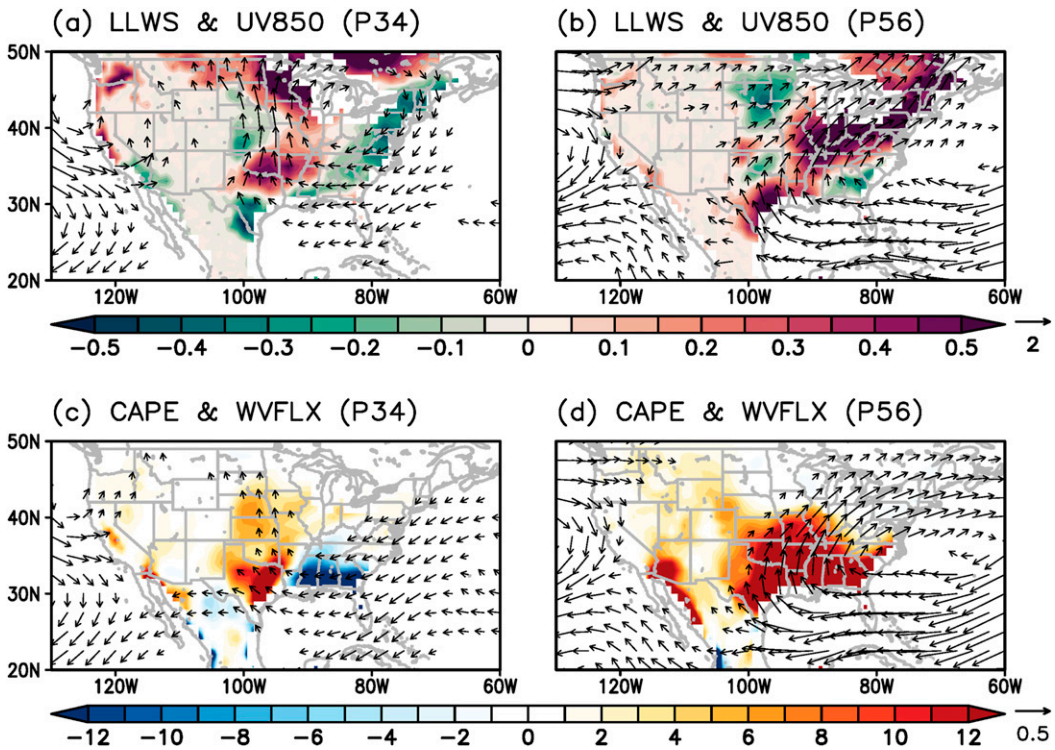

FIG. 6. Composite maps of the anomalous low-level wind shear (shaded; m s^{-1}) and wind anomalies at 850 hPa (vectors; m s^{-1}; omitted below 0.5 m s^{-1}) during (a) MJO P34 and (b) MJO P56. (c),(d) As in (a) and (b), but for the anomalous CAPE) (shaded; J kg^{-1}) and anomalous vertical integrated water vapor flux (vectors; kg m^{-1} s^{-1}; omitted below 0.1 kg m^{-1} s^{-1}). The results are derived from NARR.

Zhang and Dong 2004). Meanwhile, in boreal late spring to summer, the MJO signal is present not only over the Maritime Continent, but also over the northeast Pacific (Figs. 1c–f and Kim et al. 2014). More specifically, during MJO P3456, negative OLR anomalies occur over the Maritime Continent both in boreal winter and late spring to summer. However, the positive OLR anomalies that appear over the northeast Pacific in boreal late spring to summer are almost negligible in boreal winter. This clear distinction of the MJO-induced convection over the northeast Pacific between boreal winter and late spring to summer may aid in understanding why the MJO–U.S. tornadogenesis relationship is robust mainly in MJJ.

We carry out several LBM experiments geared toward understanding whether and how the MJO-induced anomalous diabatic heating over the Maritime Continent and cooling over the northeast Pacific modulate large-scale atmospheric circulation patterns conducive for U.S. tornadogenesis. The first LBM experiment is performed by prescribing both the diabatic heating (red contours) over the Maritime Continent (0°–10°N, 90°–150°E) and cooling (blue contours) over the northeast Pacific (5°–20°N, 70°–110°W) as shown in Fig. 7b. This experiment is referred to as the ''ALL forcings'' experiment and should aid to test whether the LBM can reproduce the observed atmospheric circulation anomalies during MJO P3456. In this and other LBM experiments, the three-dimensional background atmospheric states are prescribed using MJJ fields averaged for the period of 1979–2016 and derived from NCEP2. The magnitude of the diabatic heating is set to 3 K day^{-1}, which is derived based on the rainfall anomalies averaged over the Maritime Continent (Ting and Yu 1998). The magnitude of the diabatic cooling is set to −1.5 K day^{-1}, which roughly corresponds to the rainfall anomalies averaged over the northeast Pacific. The heating and cooling profiles are idealized to have their maximum values at the midlevel near 500 hPa, with a Gaussian distribution for both vertical and horizontal directions.

Figure 7c shows the midlevel (500 hPa) geopotential height anomaly (shaded) response to diabatic forcing (contours) in the ALL forcings experiment. Overall, the spatial patterns of midlevel geopotential height anomalies in ALL forcings experiment are largely consistent with those derived from NCEP2 (Fig. 7a), except for the anomalous anticyclone over the North Pacific, which is much weaker in the model experiment. In addition, the anomalous midlevel trough over the Gulf of Alaska and

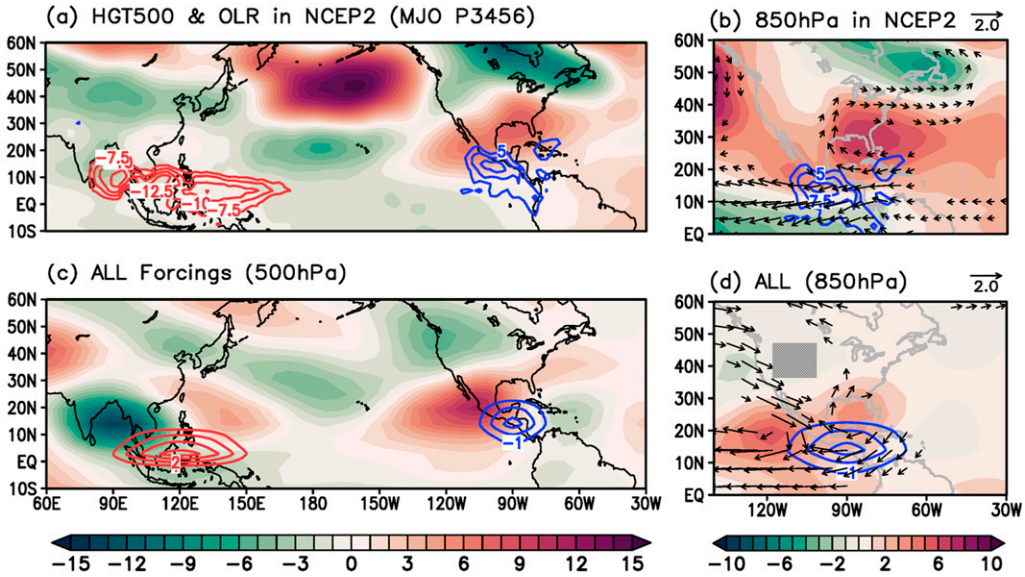

FIG. 7. (a) Anomalous geopotential height at 500 hPa (shaded; gpm) and outgoing longwave radiation (red contours for $\leq -5\ \mathrm{W\,m^{-2}}$; blue contours for $\geq +5\ \mathrm{W\,m^{-2}}$) and (b) low-level geopotential height (shaded; gpm) and wind anomalies (vectors; $\mathrm{m\,s^{-1}}$; omitted below $0.5\ \mathrm{m\,s^{-1}}$) during MJO P3456 derived from NCEP2. (c) Simulated geopotential height anomaly at 500 hPa (shaded; gpm) and (d) geopotential height anomaly (shaded; gpm) and wind anomalies at 850 hPa (vectors; $\mathrm{m\,s^{-1}}$; omitted below $0.5\ \mathrm{m\,s^{-1}}$) with the anomalous diabatic heating over the Maritime Continents (red contours; K $\mathrm{day^{-1}}$) and the anomalous diabatic cooling over the northeast Pacific (blue contours; K $\mathrm{day^{-1}}$) in the ALL forcing experiment.

the anomalous midlevel ridge centered over the southern United States are well reproduced in the ALL forcings experiment, although they are slightly shifted westward compared to NCEP2. At the low level (Figs. 7b,d), both NCEP2 and the ALL forcings experiment show the atmospheric ridge over the southern United States with the anticyclonic circulation anomalies, which in turn enhance NALLJ. In general, the results shown in Figs. 7c,d suggest that the MJO-induced anomalous diabatic forcing over the Maritime Continent and northeast Pacific can drive the observed anomalous mid- and low-level geopotential heights and winds over the Pacific and North America (Figs. 7a,b).

However, the results from the ALL forcings experiment do not explain which diabatic forcing is more important in generating the anomalous atmospheric ridge over the southern United States, which is the key factor that enhances the NALLJ and tornadic environmental parameters. To address this question, we carry out two additional LBM experiments. In one experiment, only the diabatic heating over the Maritime Continent is prescribed (i.e., the "MC forcing" experiment), whereas in the other experiment, only the diabatic cooling over the northeast Pacific is prescribed (i.e., the "EP forcing" experiment).

Figures 8a and 8b show the anomalous midlevel geopotential height, low-level geopotential height, and winds in the MC forcing experiment. The diabatic heating over the Maritime Continent generates a negative midlevel geopotential height anomaly over the Bay of Bengal. The pair of an anomalous anticyclone over the South China Sea (8°–30°N, 110°–150°E) and an anomalous cyclone across the East Asia is an extratropical stationary Rossby wave response to the diabatic heating over the Maritime Continent, as documented in Wang et al. (2001). Interestingly, the impact of the Maritime Continent diabatic heating on the mid- and low-level atmospheric circulations east of the date line is very weak. This is because the Pacific jet in MJJ is too weak and shifted too far poleward to host a robust extratropical Rossby wave response to tropical diabatic heating anomalies (e.g., Lee et al. 2009). Therefore, we can conclude that the diabatic heating over the Maritime Continent is not the leading factor that modulates U.S. tornadic environmental parameters in MJJ.

Despite the weaker diabatic forcing compared to the MC forcing experiment, the EP forcing experiment shows a robust pattern of anomalous midlevel atmospheric circulation appearing over the North Pacific and North America, largely consistent with the ALL forcings experiment (Fig. 8c). In particular, an anomalous midlevel atmospheric trough appears over the Gulf of Alaska and Canada, and a ridge appears over the southern United States. The anomalous atmospheric

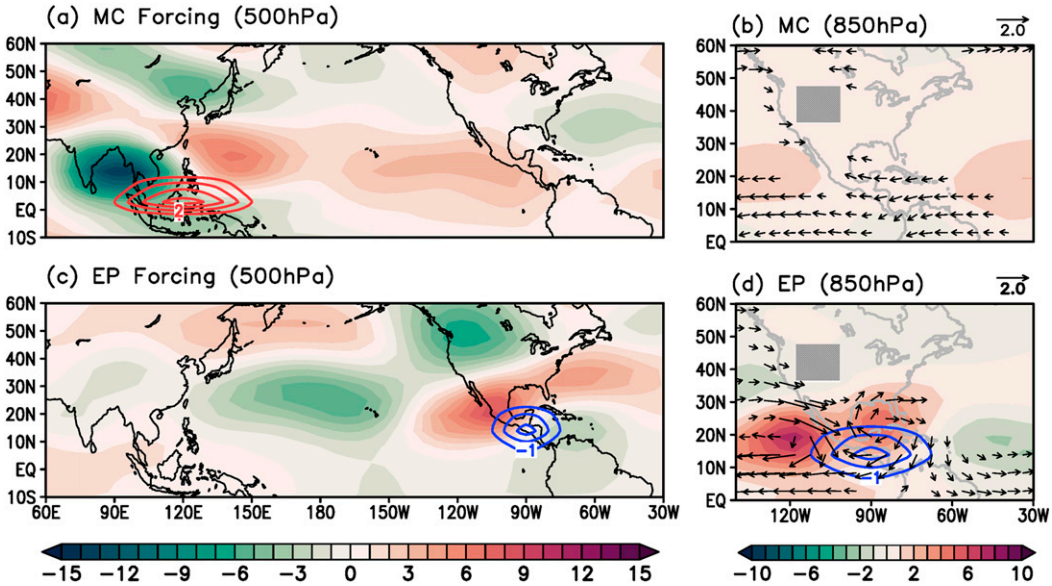

FIG. 8. (a) Simulated geopotential height anomaly at 500 hPa (shaded; gpm) and (b) geopotential height (shaded; gpm) and wind anomalies at 850 hPa (vectors; m s^{-1}; omitted below 0.5 m s^{-1}) with the anomalous diabatic heating over the Maritime Continents (red contours; K) in the MC forcing experiment. (c),(d) As in (a) and (b), but with the anomalous diabatic cooling (blue contours; K) over the northeast Pacific in the EP forcing experiment.

ridge with low-level anticyclone circulations across the northeast Pacific and southern United States appear to be a combined effect of Gill-type response (Gill 1980) and barotropic stationary Rossby wave response (e.g., Lee et al. 2009) to the diabatic cooling over the northeast Pacific (Fig. 8d). However, it should be noted that the results from the ALL forcings and EP forcing experiments (Figs. 7d and 8d) show much stronger low-level Gill-type response over the northeast Pacific than those derived from NCEP2 (Fig. 7b). Thus, it appears that the atmospheric ridge over the southern United States is largely a barotropic stationary Rossby wave response to the anomalous diabatic cooling over EP, which is the major forcing to enhance NALLJ. The anomalous atmospheric trough over Canada is an extratropical stationary Rossby response to the northeast Pacific cooling (e.g., Lee et al. 2009). The anomalous atmospheric circulations over the North Pacific appear to be a response to compensate for the mass imbalance caused by the anomalous atmospheric circulations over North America. These results strongly suggest that the MJO-induced diabatic cooling over the northeast Pacific is the key driver of the atmospheric circulations conducive for U.S. tornadogenesis.

4. Summary and discussion

Tornado occurrence is strongly controlled by synoptic-scale, mesoscale, and local atmospheric conditions. However, recent studies have shown that remote forcing such as the MJO modulates U.S. tornado activity at the subseasonal time scale (e.g., Thompson and Roundy 2013; Barrett and Gensini 2013; Tippett 2018; Baggett et al. 2018). Although previous studies have demonstrated a robust statistical relationship between MJO and U.S. tornado activity, the underlying physical mechanism for the MJO–U.S. tornadogenesis relationship has not been fully demonstrated. In this study, we first show that MJO-induced U.S. tornadogenesis is most robust in MJJ. The frequency of U.S. tornadogenesis in MJJ increases during MJO P3456, when deep tropical convection is enhanced over the Maritime Continent and suppressed over the northeast Pacific. In contrast, the frequency of U.S. tornadogenesis in MJJ decreases during MJO P1278, when the convective anomalies are nearly opposite to those during MJO P3456. Then we carry out several LBM experiments to find the physical processes linking the MJO-induced diabatic heating anomalies to U.S. tornadic environmental conditions, which are briefly summarized as a schematic in Fig. 9.

During MJO P3456, anomalous diabatic heating over the Maritime Continent induces anomalous upper-level divergence, which in turn produces anomalous upper-level convergence over the northeast Pacific through anomalous Pacific Walker circulations. This in turn produces anomalous subsidence and diabatic cooling over the northeast Pacific, forcing an anomalous

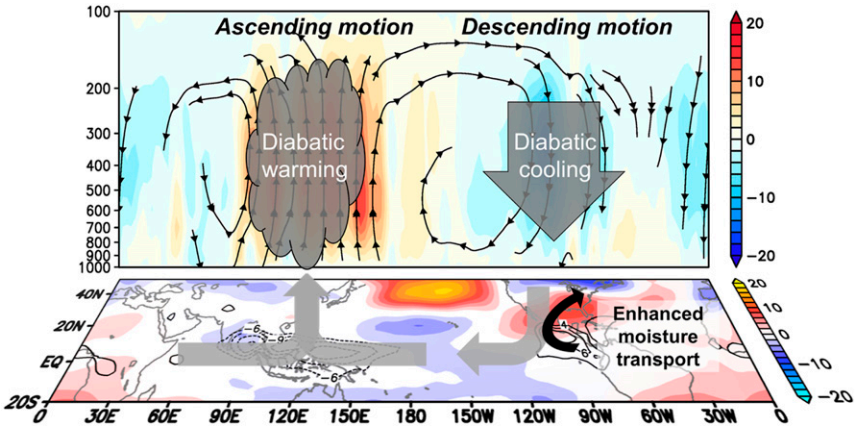

FIG. 9. (top) Schematic of spatially averaged (0°–10°N) anomalous vertical motion (omega; positive value is ascending motion; shaded; 800 Pa s^{-1}) and velocity anomaly (streamlines) during MJO P3456. (bottom) Anomalous geopotential height at 500 hPa (shaded; gpm) and OLR anomalies (contours; W m^{-2}) during MJO P3456.

atmospheric ridge with a low-level anticyclonic circulation over the southern United States through a combination of Gill-type and barotropic stationary wave responses. The low-level southerly wind anomalies associated with the anomalous anticyclone reinforces the NALLJ, increasing LLWS and CAPE, thus destabilizing the atmosphere. In summary, the MJO-induced diabatic cooling over the northeast Pacific modulates the atmospheric conditions conducive for U.S. tornadogenesis. In contrast, the MJO-induced diabatic heating over the Maritime Continent has little impact on the atmospheric conditions over the United States. Given that current state of the art seasonal forecast models have a reliable MJO forecast skill up to 30 days (e.g., Vitart 2017; Kim et al. 2018), the findings of this study may help to extend U.S. tornado forecast lead time to subseasonal time scale.

The physical mechanism proposed in this study cannot explain the MJO–U.S. tornadogenesis relationship in the boreal early and middle spring months (March and April). Compared to MJJ, the Pacific jet is strengthened and shifted southward in March and April, but the anomalous subsidence over the northeast Pacific is very weak in March and April. Therefore, it is more likely that the relationship between MJO and U.S. tornadic environmental parameters in March and April is largely influenced by extratropical stationary Rossby waves forced by MJO-induced diabatic heating anomalies over the Maritime Continent. Thus, it is also likely that natural atmospheric variabilities originated from high latitudes such as North Atlantic Oscillation (e.g., Lin et al. 2009) and Artic Oscillation (e.g., Zhou and Miller 2005) interfere with the MJO-induced extratropical teleconnection to the United States in March and April, and thus may weaken the relationship between MJO and U.S. tornadogenesis. Additionally, in March and April, tropical Pacific sea surface temperature anomalies associated with El Niño–Southern Oscillation (ENSO) are of key importance in modulating the spatiotemporal variability of U.S. tornadogenesis (e.g., Weaver et al. 2012; Lee et al. 2013, 2016; Barrett and Gensini 2013; Allen et al. 2015; Lepore et al. 2017; Molina et al. 2018; Chu et al. 2019).

Previous studies have shown that the amplitude and propagation speed of MJO as well as MJO-induced atmospheric teleconnection are considerably modulated by the background state of the ENSO (e.g., Kessler 2001; Hendon et al. 2007; Pohl and Matthews 2007; Moon et al. 2011; Wei and Ren 2019). More specifically, during El Niño, the MJO convection over the Pacific propagates farther eastward and its phase speed increases due to an expanded western Pacific warm pool (e.g., Kessler 2001; Pohl and Matthews 2007; Wei and Ren 2019). This suggests that the ENSO–MJO interaction could modulate the MJO–U.S. tornadogenesis relationship. Therefore, the interactive ENSO–MJO impact on U.S. tornadogenesis is a crucial component to fill the gap between subseasonal and seasonal U.S. tornado predictability.

Acknowledgments. We thank Jun Zhang for helpful comments and suggestions. Dongmin Kim was supported under the auspices of the Cooperative Institute for Marine and Atmospheric Studies (CIMAS), a cooperative institute of the University of Miami and NOAA, Cooperative Agreement NA10OAR4320143. This work was supported by NOAA CPO (NA12OAR4310083, GC16-207) and by NOAA CPC (N8R1MP1P00) and NOAA's Atlantic Oceanographic and Meteorological Laboratory.

REFERENCES

Allen, J. T., M. K. Tippett, and A. H. Sobel, 2015: Influence of the El Niño/Southern Oscillation on tornado and hail frequency in the United States. *Nat. Geosci.*, **8**, 278–283, https://doi.org/10.1038/ngeo2385.

Baggett, C. F., K. M. Nardi, S. J. Childs, S. N. Zito, E. A. Barnes, and E. D. Maloney, 2018: Skillful subseasonal forecasts of weekly tornado and hail activity using the Madden-Julian Oscillation. *J. Geophys. Res. Atmos.*, **123**, 12 661–12 675, https://doi.org/10.1029/2018JD029059.

Barrett, B. S., and V. A. Gensini, 2013: Variability of central United States April-May tornado day likelihood by phase of the Madden-Julian Oscillation. *Geophys. Res. Lett.*, **40**, 2790–2795, https://doi.org/10.1002/grl.50522.

——, and B. N. Henley, 2015: Intraseasonal variability of hail in the contiguous United States: Relationship to the Madden–Julian oscillation. *Mon. Wea. Rev.*, **143**, 1086–1103, https://doi.org/10.1175/MWR-D-14-00257.1.

Becker, E. J., E. H. Berbery, and R. W. Higgins, 2011: Modulation of cold-season U.S. daily precipitation by the Madden–Julian oscillation. *J. Climate*, **24**, 5157–5166, https://doi.org/10.1175/2011JCLI4018.1.

Chu, J.-E., A. Timmermann and J.-Y. Lee, 2019: North American April tornado occurrences linked to global sea surface temperature anomalies. *Sci. Adv.*, **5**, eaaw9950, https://doi.org/10.1126/sciadv.aaw9950.

Doswell, C. A., and L. F. Bosart, 2001: Extratropical synoptic-scale processes and severe convection. *Severe Convective Storms, Meteor. Monogr.*, No. 50, Amer. Meteor. Soc., 27–70, https://doi.org/10.1175/0065-9401-28.50.27.

——, H. E. Brooks, and N. Dotzek, 2009: On the implementation of the enhanced Fujita scale in the USA. *Atmos. Res.*, **93**, 554–563, https://doi.org/10.1016/j.atmosres.2008.11.003.

Gensini, V. A., and A. Marinaro, 2016: Tornado frequency in the United States related to global relative angular momentum. *Mon. Wea. Rev.*, **144**, 801–810, https://doi.org/10.1175/MWR-D-15-0289.1.

——, D. Gold, J. T. Allen, and B. S. Barrett, 2019: Extended U.S. tornado outbreak during late May 2019: A forecast of opportunity. *Geophys. Res. Lett.*, **46**, 10 150–10 158, https://doi.org/10.1029/2019GL084470.

Gill, A. E., 1980: Some simple solutions for heat-induced tropical circulation. *Quart. J. Roy. Meteor. Soc.*, **106**, 447–462, https://doi.org/10.1002/qj.49710644905.

Henderson, S. A., E. D. Maloney, and S. Son, 2017: Madden–Julian oscillation Pacific teleconnections: The impact of the basic state and MJO representation in general circulation models. *J. Climate*, **30**, 4567–4587, https://doi.org/10.1175/JCLI-D-16-0789.1.

Hendon, H. H., M. C. Wheeler, and C. Zhang, 2007: Seasonal dependence of the MJO–ENSO relationship. *J. Climate*, **20**, 531–543, https://doi.org/10.1175/JCLI4003.1.

Hoskins, B. J., and A. J. Simmons, 1975: A multi-layer spectral model and the semi-implicit method. *Quart. J. Roy. Meteor. Soc.*, **101**, 637–655, https://doi.org/10.1002/qj.49710142918.

——, and D. J. Karoly, 1981: The steady linear response of a spherical atmosphere to thermal and orographic forcing. *J. Atmos. Sci.*, **38**, 1179–1196, https://doi.org/10.1175/1520-0469(1981)038<1179:TSLROA>2.0.CO;2.

Kanamitsu, M., W. Ebisuzaki, J. Woollen, S. Yang, J. J. Hnilo, M. Fiorino, and G. L. Potter, 2002: NCEP–DOE AMIP-II Reanalysis (R-2). *Bull. Amer. Meteor. Soc.*, **83**, 1631–1644, https://doi.org/10.1175/BAMS-83-11-1631.

Kemball-Cook, S., and B. Wang, 2001: Equatorial waves and air–sea interaction in the boreal summer intraseasonal oscillation. *J. Climate*, **14**, 2923–2942, https://doi.org/10.1175/1520-0442(2001)014<2923:EWAASI>2.0.CO;2.

Kessler, W. S., 2001: EOF representation of the Madden–Julian oscillation and its connection with ENSO. *J. Climate*, **14**, 3055–3061, https://doi.org/10.1175/1520-0442(2001)014<3055:EROTMJ>2.0.CO;2.

Kim, D., M.-I. Lee, H.-M. Kim, and S. D. Schubert, 2014: The modulation of tropical storm activity in the western North Pacific by the Madden-Julian Oscillation in the GEOS-5 AGCM experiments. *Atmos. Sci. Lett.*, **15**, 335–341, https://doi.org/10.1002/asl2.509.

Kim, H., F. Vitart, and D. E. Waliser, 2018: Prediction of the Madden–Julian oscillation: A review. *J. Climate*, **31**, 9425–9443, https://doi.org/10.1175/JCLI-D-18-0210.1.

Lawrence, D. M., and P. J. Webster, 2002: The boreal summer intraseasonal oscillation: Relationship between northward and eastward movement of convection. *J. Atmos. Sci.*, **59**, 1593–1606, https://doi.org/10.1175/1520-0469(2002)059<1593:TBSIOR>2.0.CO;2.

Lee, M.-I., H.-S. Kang, D. Kim, D. Kim, H. Kim, and D. Kang, 2014: Validation of the experimental hindcasts produced by the GloSea4 seasonal prediction system. *Asia-Pac. J. Atmos. Sci.*, **50**, 307–326, https://doi.org/10.1007/s13143-014-0019-4.

Lee, S.-K., C. Wang, and B. E. Mapes, 2009: A simple atmospheric model of the local and teleconnection responses to tropical heating anomalies. *J. Climate*, **22**, 272–284, https://doi.org/10.1175/2008JCLI2303.1.

——, R. Atlas, D. B. Enfield, C. Wang, and H. Liu, 2013: Is there an optimal ENSO pattern that enhances large-scale atmospheric processes conducive to major tornado outbreaks in the United States? *J. Climate*, **26**, 1626–1642, https://doi.org/10.1175/JCLI-D-12-00128.1.

——, A. T. Wittenberg, D. B. Enfield, S. J. Weaver, C. Wang, and R. Atlas, 2016: U.S. regional tornado outbreaks and their links to ENSO phases and North Atlantic SST variability. *Environ. Res. Lett.*, **11**, 044008, https://doi.org/10.1088/1748-9326/11/4/044008.

Lepore, C., M. K. Tippett, and J. T. Allen, 2017: ENSO-based probabilistic forecasts of March–May U.S. tornado and hail activity. *Geophys. Res. Lett.*, **44**, 9093–9101, https://doi.org/10.1002/2017GL074781.

Liebmann, B., and C. A. Smith, 1996: Description of a complete (interpolated) outgoing longwave radiation dataset. *Bull. Amer. Meteor. Soc.*, **77**, 1275–1277.

Lin, H., G. Brunet, and J. Derome, 2009: An observed connection between the North Atlantic Oscillation and the Madden–Julian oscillation. *J. Climate*, **22**, 364–380, https://doi.org/10.1175/2008JCLI2515.1.

Lopez, H., S.-K. Lee, S. Dong, G. Goni, B. Kirtman, R. Atlas, and A. Kumar, 2019: East Asian monsoon as a modulator of U.S. Great Plains heat waves. *J. Geophys. Res. Atmos.*, **124**, 6342–6358, https://doi.org/10.1029/2018JD030151.

Madden, R. A., and P. R. Julian, 1972: Description of global-scale circulation cells in the tropics with a 40–50 day period. *J. Atmos. Sci.*, **29**, 1109–1123, https://doi.org/10.1175/1520-0469(1972)029<1109:DOGSCC>2.0.CO;2.

Mesinger, F., and Coauthors, 2006: North American Regional Reanalysis. *Bull. Amer. Meteor. Soc.*, **87**, 343–360, https://doi.org/10.1175/BAMS-87-3-343.

Molina, M. J., and J. T. Allen, 2019: On the moisture origins of tornadic thunderstorms. *J. Climate*, **32**, 4321–4346, https://doi.org/10.1175/JCLI-D-18-0784.1.

——, ——, and V. A. Gensini, 2018: The Gulf of Mexico and ENSO influence on subseasonal and seasonal CONUS winter tornado variability. *J. Appl. Meteor. Climatol.*, **57**, 2439–2463, https://doi.org/10.1175/JAMC-D-18-0046.1.

Moon, J.-Y., B. Wang, and K.-J. Ha, 2011: ENSO regulation of MJO teleconnection. *Climate Dyn.*, **37**, 1133–1149, https://doi.org/10.1007/s00382-010-0902-3.

Moore, T. W., and M. P. McGuire, 2020: Tornado-days in the United States by phase of the Madden–Julian oscillation and global wind oscillation. *Climate Dyn.*, **54**, 17–36, https://doi.org/10.1007/s00382-019-04983-y.

Pohl, B., and A. J. Matthews, 2007: Observed changes in the lifetime and amplitude of the Madden–Julian oscillation associated with interannual ENSO sea surface temperature anomalies. *J. Climate*, **20**, 2659–2674, https://doi.org/10.1175/JCLI4230.1.

Thompson, D. B., and P. E. Roundy, 2013: The relationship between the Madden–Julian oscillation and U.S. violent tornado outbreaks in the spring. *Mon. Wea. Rev.*, **141**, 2087–2095, https://doi.org/10.1175/MWR-D-12-00173.1.

Ting, M., and I. M. Held, 1990: The stationary wave response to tropical SST anomaly in an idealized GCM. *J. Atmos. Sci.*, **47**, 2546–2566, https://doi.org/10.1175/1520-0469(1990)047<2546:TSWRTA>2.0.CO;2.

——, and L. Yu, 1998: Steady response to tropical heating in wavy linear and nonlinear baroclinic models. *J. Atmos. Sci.*, **55**, 3565–3582, https://doi.org/10.1175/1520-0469(1998)055<3565:SRTTHI>2.0.CO;2.

Tippett, M. K., 2018: Robustness of relations between the MJO and U.S. tornado occurrence. *Mon. Wea. Rev.*, **146**, 3873–3884, https://doi.org/10.1175/MWR-D-18-0207.1.

Verbout, S. M., H. E. Brooks, L. M. Leslie, and D. M. Schultz, 2006: Evolution of the U.S. tornado database: 1954–2003. *Wea. Forecasting*, **21**, 86–93, https://doi.org/10.1175/WAF910.1.

Vitart, F., 2017: Madden–Julian oscillation prediction and teleconnections in the S2S database. *Quart. J. Roy. Meteor. Soc.*, **143**, 2210–2220, https://doi.org/10.1002/qj.3079.

Wang, B., R. Wu, and K. Lau, 2001: Interannual variability of the Asian summer monsoon: Contrasts between the Indian and the western North Pacific–East Asian monsoons. *J. Climate*, **14**, 4073–4090, https://doi.org/10.1175/1520-0442(2001)014<4073:IVOTAS>2.0.CO;2.

Wang, H., and R. Fu, 2004: Influence of cross-Andes flow on the South American low-level jet. *J. Climate*, **17**, 1247–1262, https://doi.org/10.1175/1520-0442(2004)017<1247:IOCFOT>2.0.CO;2.

Watanabe, M., and M. Kimoto, 1999: Tropical-extratropical connection in the Atlantic atmosphere-ocean variability. *Geophys. Res. Lett.*, **26**, 2247–2250, https://doi.org/10.1029/1999GL900350.

Weaver, S. J., S. Baxter, and A. Kumar, 2012: Climatic role of North American low-level jets on U.S. regional tornado activity. *J. Climate*, **25**, 6666–6683, https://doi.org/10.1175/JCLI-D-11-00568.1.

Wei, Y., and H. Ren, 2019: Modulation of ENSO on fast and slow MJO modes during boreal winter. *J. Climate*, **32**, 7483–7506, https://doi.org/10.1175/JCLI-D-19-0013.1.

Wheeler, M. C., and H. H. Hendon, 2004: An all-season real-time multivariate MJO index: Development of an index for monitoring and prediction. *Mon. Wea. Rev.*, **132**, 1917–1932, https://doi.org/10.1175/1520-0493(2004)132<1917:AARMMI>2.0.CO;2.

Zhang, C., and M. Dong, 2004: Seasonality in the Madden–Julian oscillation. *J. Climate*, **17**, 3169–3180, https://doi.org/10.1175/1520-0442(2004)017<3169:SITMO>2.0.CO;2.

Zhou, S., and A. J. Miller, 2005: The interaction of the Madden–Julian oscillation and the Arctic Oscillation. *J. Climate*, **18**, 143–159, https://doi.org/10.1175/JCLI3251.1.

——, M. L'Heureux, S. Weaver, and A. Kumar, 2012: A composite study of the MJO influence on the surface air temperature and precipitation over the continental United States. *Climate Dyn.*, **38**, 1459–1471, https://doi.org/10.1007/s00382-011-1001-9.